

RAPID: Reconfigurable, Adaptive Platform for Iterative Design

Zi Yin* Fanhong Li* Shurui Zheng Jia Liu†
Tsinghua University

*Equal Contribution †Corresponding Author

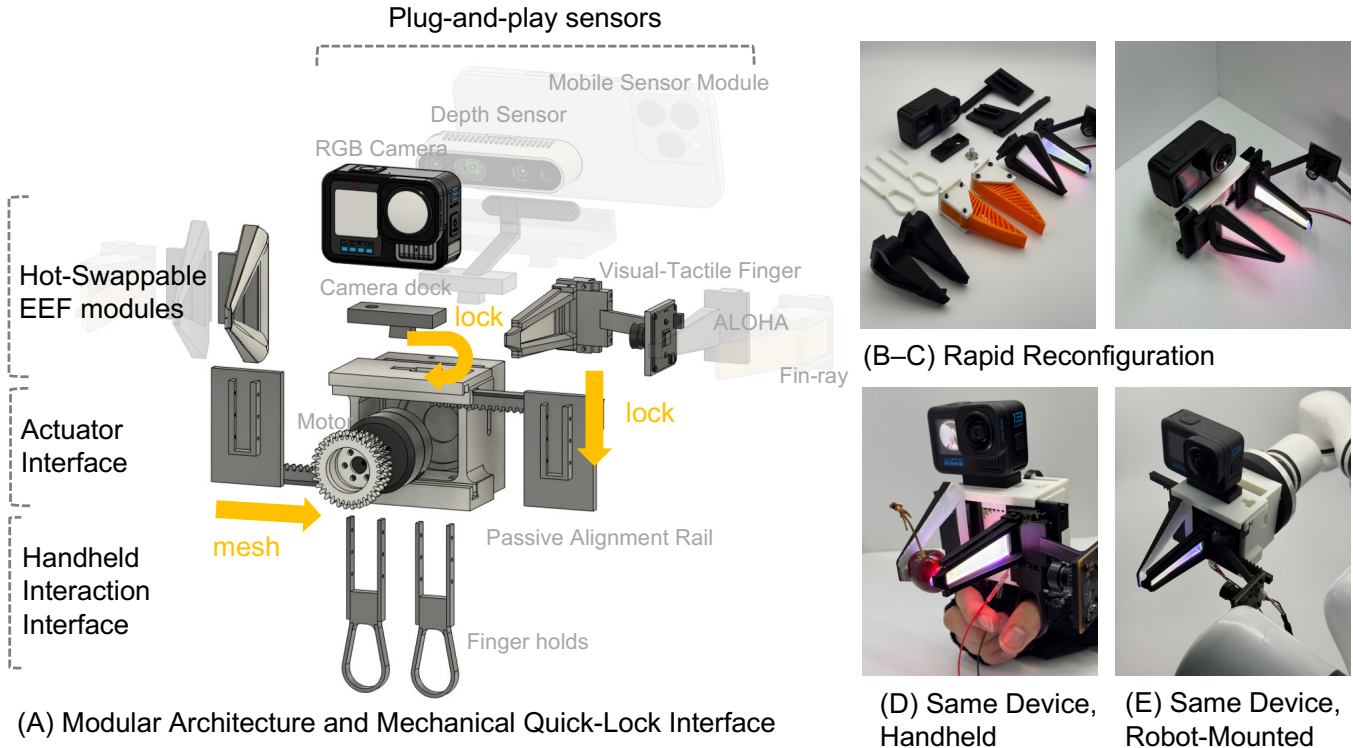


Fig. 1. RAPID system overview. RAPID is a reconfigurable robotic platform enabling tool-free, plug-and-play integration of sensors, hot-swappable end-effectors, and modular actuation. The same modular device supports both handheld data collection and robot-mounted deployment through rapid physical reconfiguration.

Abstract—Developing robotic manipulation policies is iterative and hypothesis-driven: researchers test tactile sensing, gripper geometries, and sensor placements through real-world data collection and training. Yet even minor end-effector changes often require mechanical refitting and system re-integration, slowing iteration. We present RAPID, a full-stack reconfigurable platform designed to reduce this friction. RAPID is built around a tool-free, modular hardware architecture that unifies handheld data collection and robot deployment, and a matching software stack that maintains real-time awareness of the underlying hardware configuration through a driver-level *Physical Mask* derived from USB events. This modular hardware architecture reduces reconfiguration to seconds and makes systematic multi-modal ablation studies practical, allowing researchers to sweep diverse gripper and sensing configurations without repeated system bring-up. The Physical Mask exposes modality presence as an explicit runtime signal, enabling auto-configuration and graceful degradation under sensor hot-plug events, so policies can continue executing when sensors are physically added or removed. System-centric experiments show that RAPID reduces

the setup time for multi-modal configurations by two orders of magnitude compared to traditional workflows and preserves policy execution under runtime sensor hot-unplug events. The hardware designs, drivers, and software stack are open-sourced at <https://rapid-kit.github.io/>.

I. INTRODUCTION

Learning robotic manipulation policies from demonstrations is increasingly an iterative, hypothesis-driven process: researchers test whether tactile sensing helps on fragile objects, whether wider fingers reduce failures, or whether alternative sensor placements improve observability in clutter [13, 53]. At the same time, the community has moved beyond visual-only imitation to multi-modal interfaces that combine vision, proprioception, and touch, often utilizing portable handheld grippers for in-the-wild data collection [14, 46, 19, 51].

These handheld interfaces, from UMI and its variants [14, 52, 48, 12, 37, 20] to low-cost teleoperation systems [46,

19, 51], have significantly broadened where and how we can collect demonstrations. However, as sensing and embodiment options proliferate, they also amplify a more mundane but critical bottleneck: every new gripper geometry, fingertip material, or sensor combination often means a new round of mechanical refitting and software integration before any data can be collected. In a typical study, characterizing the benefit of tactile sensing across different object geometries might require testing N gripper designs against M sensor configurations. Under a traditional workflow—typically involving screw-based end-effector swaps, manual configuration edits, and repeated restarts of the logging stack—systematically exploring this $N \times M$ space is prohibitively expensive.

We argue that to accelerate multi-modal manipulation research, we must transition from static interfaces to *full-stack reconfigurable platforms*. In our experience, such a platform must solve two coupled problems: (i) the *mechanical friction* of swapping components, so that changing end-effectors, fingertips, or sensor modules becomes a seconds-level operation rather than minutes of bespoke rework; and (ii) the *modality observability gap*, namely the fact that the software stack has no principled way to know which sensing and actuation channels are physically present at a given moment, and therefore cannot safely adapt when sensors are added or removed.

We present RAPID (Reconfigurable, Adaptive Platform for Multi-Modal Iterative Design), a full-stack platform designed to reduce this iteration gap. RAPID is built around two pillars: (1) a tool-free, modular hardware architecture that unifies handheld data collection and robot-mounted deployment, allowing researchers to sweep across diverse gripper and sensing configurations without repeated system bring-up; and (2) a matching software stack that maintains real-time awareness of the underlying hardware configuration through a driver-level *Physical Mask* derived from USB hot-plug events.

At the software level, the Physical Mask exposes modality presence as an explicit runtime signal: at any time step, the system knows which modalities (e.g., wrist camera, visuotactile fingertip, torque sensing) are physically online, based on USB connect and disconnect events. This hardware-grounded signal complements training-time modality dropout [34, 27]. While dropout encourages policies to be robust to missing inputs at the representation level, the Physical Mask provides the system-level observability needed to auto-configure logging and to gracefully degrade policy execution when sensors are hot-plugged, allowing policies to continue executing when sensors are physically added or removed.

We evaluate RAPID through a system-centric lens, focusing on iteration overhead and runtime robustness rather than task-specific success rates. We quantify the time savings enabled by our tool-free design and auto-discovery pipeline in a representative multi-modal ablation scenario, and we probe runtime behavior by physically unplugging and re-plugging sensors during a tactile identification task. Our contributions are three-fold:

- **A full-stack reconfigurable manipulation platform** that unifies handheld data collection and robot-mounted

deployment through a tool-free, modular hardware architecture and a unified I/O stack.

- **A driver-level Physical Mask abstraction** that derives modality presence from USB events and exposes it as an explicit runtime signal, enabling auto-configuration and graceful degradation under sensor hot-plug events.
- **A system-centric evaluation** demonstrating that RAPID reduces the setup time for multi-modal configurations by two orders of magnitude compared to traditional workflows, and preserves policy execution under runtime sensor hot-unplug scenarios.

II. RELATED WORK

A. Portable Manipulation Interfaces and Hardware Fragmentation

The Universal Manipulation Interface (UMI) [14] established a paradigm shift in robot learning by enabling handheld, vision-based data collection without requiring the target robot during demonstration. This approach decouples demonstration capture from robot hardware, allowing “in-the-wild” data collection that has driven significant progress in imitation learning [13, 53].

The success of UMI has spurred a family of specialized variants, each addressing specific limitations. FastUMI [52] replaced offline visual SLAM with onboard Visual-Inertial Odometry using the Intel RealSense T265 to streamline tracking, though this introduced data format incompatibilities. Dex-UMI [48] extended the concept to wearable hand exoskeletons, while TacUMI [12] integrated force-torque sensing and visuotactile fingertips, replacing the GoPro SLAM approach with HTC Vive external tracking to obtain *interference-free* data. Other specialized variants include ExUMI [49] for proprioception via magnetic encoders, MV-UMI [37] for multi-view capture, and UMI-on-Legs [20] for quadruped deployment. Parallel efforts like GELLO [46] and Mobile ALOHA [19, 51] have similarly advanced low-cost teleoperation.

While each variant addresses real limitations, they exist largely as *siloed designs* [5]. The same UMI concept has spawned at least five fundamentally different tracking approaches (GoPro, T265, Vive, ARKit, Quest 3), each complicating direct data interoperability. Furthermore, adding new modalities often requires complete system redesign. In contrast, RAPID is designed not as a single fixed interface but as a *full-stack reconfigurable platform* that aims to cover the continuous spectrum of configurations needed for systematic multi-modal ablation studies, while keeping the iteration friction of moving between them low.

B. Multi-Modal Integration and Runtime Observability

Integrating non-visual modalities into robot learning pipelines introduces significant system complexity. Tactile sensing improves manipulation in contact-rich tasks [25, 50, 32, 40], but current architectures often treat sensor configurations as *static assumptions*: the software expects a fixed set of sensors and fails ungracefully if one is missing [3]. This contributes to what we refer to as a *modality observability gap*:

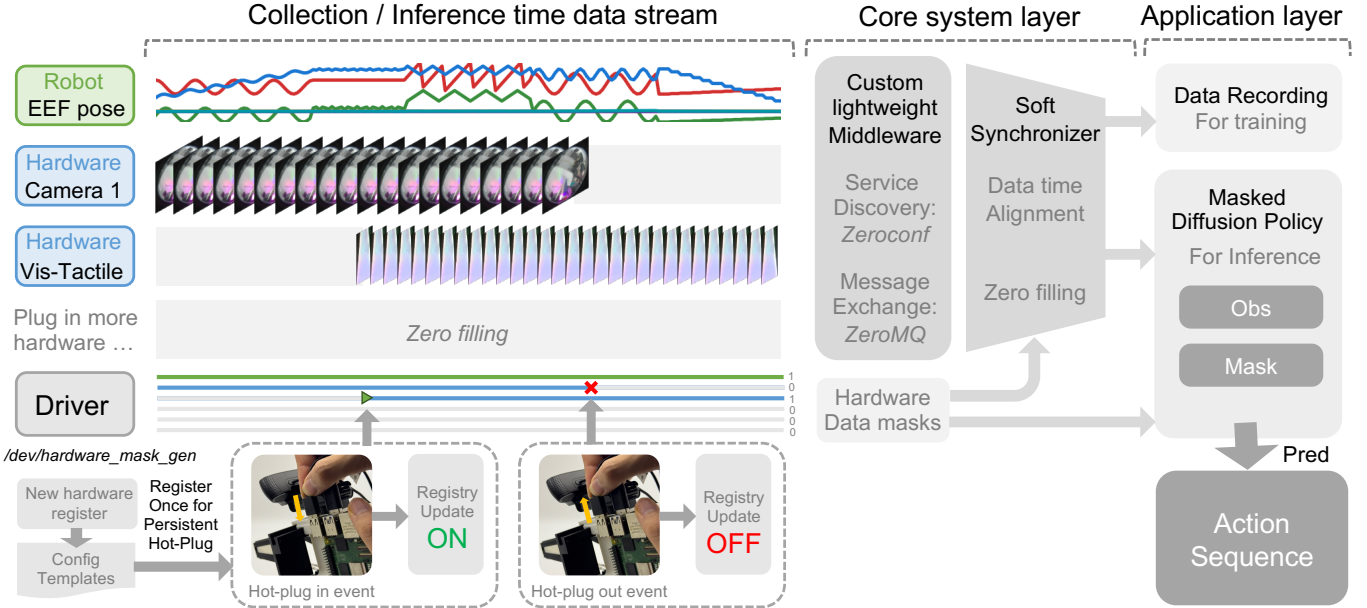


Fig. 2. Runtime architecture of the RAPID system. The top panel shows asynchronous multimodal data streams during collection and inference, including robot end-effector state, vision, tactile sensing and optional other plug-in modalities. The bottom panel illustrates the event-driven pathway from hardware hot-plug events to the driver-generated Physical Mask, which is propagated through lightweight middleware to the application layer. The Physical Mask enables time alignment and zero filling of absent modalities, ensuring fixed-dimensional observations for data recording and mask-aware policy inference.

the system has no principled way to know which modalities are physically present at a given time.

The foundational technique of modality dropout [34] and its adaptation to robotics [27] demonstrated that policies can learn robustness to sensor noise. Recent work has refined these techniques through disentangled representations (DisDP) [45], variational information bottlenecks [18], and inference-time composition (MCDP) [8]. However, these works typically assume that sensor malfunctions are already detected by the system. Current fusion architectures, such as Visuo-Tactile Transformers [11], FoAR [21], and Visual-Geometry Diffusion Policy (VGDP) [43], provide *algorithmic robustness* but do not make system-level observability of hardware a first-class concern. Similarly, runtime monitors like FIPER [38], Sentinel [1], and uncertainty detectors [47] detect policy failures but largely assume valid data flow. The closest work on graceful degradation [42] handles noisy sensors but not physical absence.

RAPID targets this system-level modality observability gap with a driver-level *Physical Mask*. Unlike timeout heuristics that infer absence from missing data, the Physical Mask is updated directly from USB connect and disconnect events, exposing modality presence as an explicit runtime signal that can drive auto-configuration and graceful degradation when sensors are hot-plugged.

C. Modular Design and Hardware Iteration Bottleneck

The theoretical motivation for hardware-software co-design is well-established [41, 9, 10]. However, co-design research is conducted almost exclusively in simulation because real-world iteration is prohibitively expensive [28, 22, 4]. The

simulation-reality gap is often non-monotonic with respect to morphology [39, 24], meaning that predicting which hardware changes will improve real-world performance requires physical experimentation [2, 23].

Existing real-world efforts face significant integration friction. While some works have explored physical evolution [6, 35, 17], manual assembly remains the bottleneck [33, 15]. Modular systems like the Yale OpenHand [29] or Fable [36] require significant reconfiguration time. Recent soft gripper systems [31] achieve fast swaps but are limited to specific actuators. RAPID adopts traditional joinery principles—specifically mortise-and-tenon joints [16, 26, 44]—and pairs them with event-driven software discovery. Our goal is not autonomous self-reconfiguration, but minimizing the *human overhead* of hardware iteration in a full-stack reconfigurable platform. By reducing per-configuration setup time from minutes to seconds, RAPID shifts the bottleneck of multi-modal ablation studies from engineering debugging back to scientific inquiry.

III. SYSTEM DESIGN

Building on the challenges identified in Section II, RAPID is built around two pillars. The first is a *tool-free, modular hardware architecture* (Section III-A) that reduces end-effector and sensor swaps to seconds-level operations and unifies handheld data collection with robot-mounted deployment. The second is a *driver-level Physical Mask* (Sections III-B-III-C) that derives modality presence from USB hot-plug events, providing the system-level observability needed for auto-configuration and graceful degradation under runtime sensor changes. Fig. 2 illustrates the resulting layered architecture.

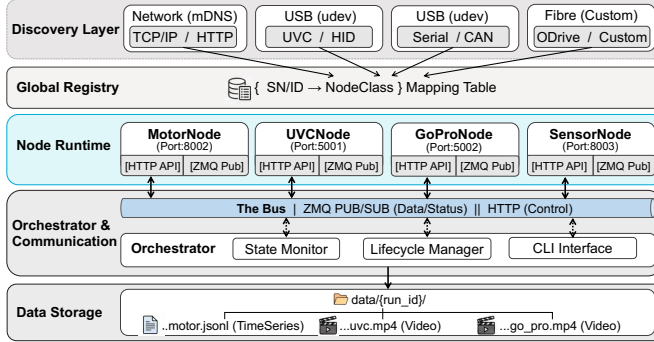


Fig. 3. System implementation of RAPID. The discovery layer supports heterogeneous device interfaces (USB-CAN, USB-Serial, USB-LAN, and native USB) through a unified hub. The driver layer performs event-driven device registration and generates the Physical Mask via a virtual device file. The middleware layer publishes sensor streams and the mask over a lightweight publish-subscribe transport (ZeroMQ + Zeroconf). The synchronisation layer aligns multimodal observations within a configurable time window and zero-fills absent channels. The application layer consumes fixed-dimension observations in either collection mode (logging with per-frame mask) or inference mode (mask-aware policy execution).

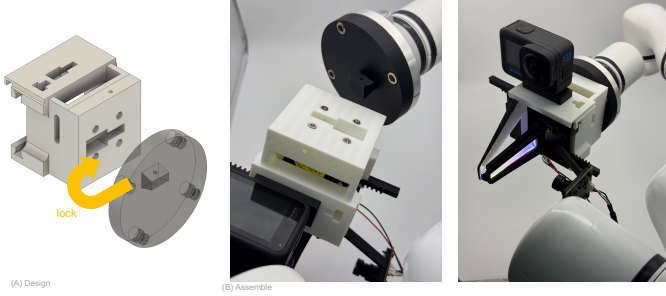


Fig. 4. Hardware layer details. (A) Tool-free connector design. (B) Rapid deployment to robot arm as end-effector.

A. Hardware Layer

The hardware layer is designed to support frequent re-configuration (Fig. 4). **Base and standardized slots.** The base is a 3D-printed chassis that integrates motor mounting and cable routing; it remains fixed across configurations. The base exposes four standardized attachment slots: front (finger bodies), tip (fingertips), top (wrist camera mounts), and bottom (handheld or robot-mounting adapters). Only modules change; the base does not. This slot-based design also enables dual-use operation: the same base hardware supports both handheld data collection and robot-mounted deployment by swapping the bottom adapter. **Mechanical attachment.** Modules connect via mortise-and-tenon joints, a geometry well-suited to FDM-printed PLA: it tolerates typical printing variation and survives repeated insertion cycles better than snap-fit alternatives. Similar joints appear in prior work, including the 3D-printed fingers of ALOHA [51] and the GET tactile fingertip [7]. For extended operation, a single set screw can be added for additional retention. **Electrical interface.** We adopt USB as a unified interconnect layer. USB offers mature hot-plug support at the OS level and a wide ecosystem of converter boards, which

simplifies replication. The system aggregates heterogeneous devices through a USB hub: USB2CAN (motors, robot arm), USB2Serial (ToF sensors), USB2LAN (LiDAR, GoPro), and native USB devices (RealSense, webcam, tactile sensors), as shown in Fig. 3. Devices with direct LAN connections are integrated through a parallel registration mechanism. The output of this layer is the USB plug/unplug event: when a module is physically inserted or removed, the operating system generates an event that propagates to the driver layer.

B. Driver Layer

The driver layer translates USB events into runtime state information for the software stack. **Event detection and device registry.** A daemon process monitors USB plug/unplug events from the operating system. Upon each event, the daemon queries a registry of known modules; if the device matches a registered module, the corresponding data node is started or stopped. Stable device paths are established via udev symlinks (e.g., `/dev/rapid/tactile_left`), using USB serial numbers when available or port topology as fallback. An orchestrator monitors node health via periodic heartbeats; failed nodes are automatically restarted with backoff. **Single-point registration.** To add a new module type, users maintain a single configuration file specifying device identifiers and data publishing logic. A registration script validates the configuration and generates all derived artifacts (udev rules, descriptor files, node entries). This keeps the user-facing configuration minimal while ensuring system-wide consistency.

Physical Mask Generator. The central contribution of this layer is a virtual device that reads the current registry state and exposes the **Physical Mask** at 500 Hz via a device file (e.g., `/dev/hardware_mask_gen`). We define the Physical Mask as a vector-valued signal that maps each modality name to a boolean indicating its current physical presence, serialized as a JSON dictionary. Unlike data-timeout heuristics, this mask reflects hardware state directly: a modality is marked absent the moment its USB disconnect event fires, not after a timeout window (Fig. 2, bottom). This real-time, hardware-grounded signal is what enables downstream layers to distinguish transient packet loss from physical removal. The output of this layer is the Physical Mask device file, continuously updated to reflect which sensing and actuation channels are physically online.

C. Middleware and Application Layer

Middleware. We implement a lightweight publish-subscribe layer based on ZeroMQ and Zeroconf, chosen over ROS2 [30] for ease of customization and deployment in rapid prototyping. The Physical Mask device file from the driver layer is published as a topic at this layer, alongside sensor data streams.

Synchronized Subscriber. A synchronized subscriber aggregates multiple data topics and the mask topic, aligning them within a configurable time window (default 25 ms, similar to ROS ApproximateSync), as illustrated in the three-layer data flow of Fig. 2 (top). When the Physical Mask indicates a modality is offline, the subscriber performs zero-filling for

that channel, ensuring downstream consumers always receive fixed-dimension input.

Dual-mode operation. The application layer supports two modes that share the same underlying infrastructure but run different programs:

- *Inference mode*: At each control step, the inference program fetches synchronized data with the current Physical Mask, then feeds both to a mask-aware multimodal Diffusion Policy [13]. Absent modalities are zero-filled to maintain fixed input dimensions; the policy uses the mask to determine which channels carry valid observations. Because the mask is hardware-grounded, sensor hot-plug does not crash the pipeline.
- *Collection mode*: The collection program displays real-time modality status (registered vs. physically present), records synchronized data streams, and logs the Physical Mask per frame. Since the mask updates at 500 Hz while data is recorded at 30–60 Hz, the mask captures transient dropouts at finer granularity than the data itself. This enables systematic reuse of partially corrupted episodes and simplifies post-hoc data auditing.

Unlike training-time dropout masks derived through post-processing, the Physical Mask is recorded as ground-truth hardware state at capture time—information rarely available in existing datasets.

IV. EVALUATION

Policy training. We use the standard CNN-based Diffusion Policy [13] with two observation modalities: a wrist camera image and a visuotactile fingertip image. During training, each modality is independently dropped with probability $p=0.3$ (subject to the constraint that at least one modality remains), and the corresponding feature embedding is zeroed. At inference time, the Physical Mask replaces random dropout: when a sensor is physically absent, the same zeroing is applied to its feature embedding, exactly matching the training-time condition.

A. Reconfiguration Efficiency

We evaluate the time savings enabled by RAPID’s design choices in a representative ablation study scenario. Consider a researcher iterating through $N=3$ gripper materials (rigid, Finray, silicone) $\times M=3$ sensor modalities (vision-only, vision+motor, vision+tactile), requiring 9 configurations total.

Table I compares the time cost under a traditional workflow versus RAPID. The traditional workflow is defined as RAPID with each design choice removed:

- Without quick-release: screw-based end-effector swap
- Without auto-discovery: manual YAML configuration editing
- Without hot-swap: restart collection system via Ctrl-C and relaunch
- Without unified hardware: separate devices for handheld collection and robot execution, requiring redundant sensor deployment

TABLE I
RECONFIGURATION TIME COMPARISON: TRADITIONAL WORKFLOW VS. RAPID FOR $N \times M=9$ CONFIGURATIONS.

Design Choice	Traditional	Δ Saved	Ours
EEF swap	Screw (5 ± 1 min)	–295 sec	Quick-release (5 sec)
Modality config	Manual YAML (2 ± 0.5 min)	–120 sec	Auto-discovery (0 sec)
Collection system	Ctrl-C + restart (30 ± 10 sec)	–30 sec	Hot-plug support (0 sec)
Sensor deployment	$\times 2$ (handheld \neq exec)	–50%	$\times 1$ (unified)
Per-config total	~480 sec	~475 sec	~5 sec
Full ablation ($N \times M=9$)	~72 min	~71 min	~45 sec

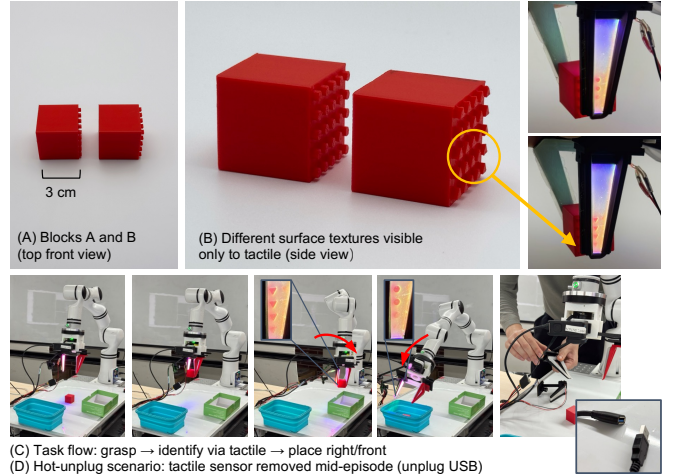


Fig. 5. Experiment task for evaluating runtime modality change. Blocks A and B appear identical to the wrist camera but differ in surface texture (triangular vs. hexagonal) perceptible through tactile sensing. The policy must grasp, identify, and place the triangular block to the left and the hexagonal block to the front. We test system behavior when the tactile sensor is unplugged during execution.

In our prototype implementation and the configuration set used in this paper, RAPID reduces per-configuration setup time from approximately 480 s to 5 s. For the full $N \times M=9$ ablation, this translates to on the order of $100\times$ speedup, shifting the practical bottleneck from interface reconfiguration back to data collection itself.

B. Inference with Runtime Modality Change

We evaluate whether the Physical Mask mechanism enables graceful degradation during inference when sensors are physically added or removed (Fig. 5). We emphasize that this experiment is not designed to benchmark manipulation performance against state-of-the-art policies, but to stress-test system behavior under runtime modality changes.

Task. The gripper is equipped with a wrist camera and a visuotactile fingertip. Two visually identical blocks (A and B) are presented; they differ only in surface texture on the side faces (one with a triangular pattern and the other with a hexagonal pattern), which is perceptible through tactile but not visual sensing. The policy must grasp each block, identify it via tactile feedback, and place the triangular block to the left and the hexagonal block to the front.

Metric. We report identification accuracy (correct placement / total trials) over 25 trials. We also report system sta-

TABLE II
INFERENCE UNDER RUNTIME MODALITY CHANGES. SCORE:
IDENTIFICATION ACCURACY OVER 25 TRIALS. STATUS: NORMAL /
DEGRADED / CRASH.

Condition	RAPID		Static Config	
	Score	Status	Score	Status
Full	0.92	Normal	0.92	Normal
No-tactile	0.52	Degraded	0.52	Degraded
Hot-unplug	0.56	Degraded	—	Crash
Hot-replug	0.84	Normal	—	Crash

tus: Normal (completed), Degraded (completed with reduced performance), or Crash (pipeline failure).

Conditions. We compare RAPID (with Physical Mask) against a baseline that uses the same hardware and policy but replaces the Physical Mask layer with a static configuration file specifying which sensors are expected. In the baseline, changing the sensor set requires manually editing this file and restarting the pipeline before execution. We test four conditions:

- *Full*: wrist camera + tactile online throughout.
- *No-tactile*: tactile absent from the start. For the baseline, the tactile entry is manually removed from the configuration file before launch.
- *Hot-unplug*: tactile physically removed mid-episode.
- *Hot-replug*: tactile removed and then reinserted mid-episode.

Results. Table II reports results per condition.

V. DISCUSSION

We presented RAPID to address the high integration friction that currently hinders systematic multi-modal ablation studies. By decoupling component exchange from system reconfiguration, RAPID shifts the bottleneck of the research loop from engineering debugging back to scientific inquiry.

A. Trade-offs of Tool-Free Modularity

A primary concern with reconfigurable hardware is the potential loss of mechanical rigidity compared to screw-based assemblies. Our use of mortise-and-tenon joints prioritizes exchange speed and 3D printing tolerance over absolute stiffness. While sufficient for the contact forces typical of handheld data collection and pick-and-place tasks, this design may introduce deflection under high-load manipulation or precision assembly tasks. For such regimes, the system supports adding a single retention screw to lock the joint, effectively trading reconfiguration speed for mechanical rigidity. This hybrid approach allows users to use the tool-free mode for rapid prototyping and the locked mode for final large-scale data collection. A more systematic characterization of this stiffness–reconfigurability trade-off, across different materials and loading regimes, is left for future work.

B. Physical Mask as a Data Curation Tool

Beyond preventing runtime crashes, the Physical Mask has broader implications for data efficiency. In traditional pipelines, episodes with missing sensor data are often discarded entirely to maintain tensor shape consistency. RAPID enables the collection and utilization of heterogeneous datasets where episodes with varying sensor availability coexist. By logging the mask alongside the trajectory, researchers can train policies that explicitly learn robustness to sensor failure or leverage expensive tactile sensors only for a subset of the data while using cheaper visual-only setups for the bulk. This capability transforms hardware failure from a fatal error into a manageable data attribute. In this sense, the Physical Mask is not only a runtime safety mechanism but also a dataset-level abstraction that supports more realistic system-centric evaluation of multimodal policies.

C. Limitations

We acknowledge several limitations in both our system implementation and experimental scope. Technically, relying on USB hubs to aggregate heterogeneous sensors introduces bandwidth constraints when operating multiple high-resolution cameras simultaneously. Furthermore, while our software synchronization is effective for standard policy learning, it lacks the microsecond-level precision of hardware-triggered synchronization required for high-speed dynamic manipulation. Experimentally, our evaluation was conducted in a single laboratory setting. While the system aims to democratize data collection, large-scale cross-institution validation is required to fully characterize reproducibility. Additionally, we do not claim state-of-the-art manipulation performance; our experiments were designed to stress-test system stability and iteration friction rather than to benchmark policy success rates against highly-tuned baselines. Moreover, while RAPID automates device discovery, the geometric alignment of newly inserted cameras still requires manual extrinsic calibration, which remains a per-reconfiguration bottleneck. Finally, the long-term durability of the PLA printed interfaces under thousands of insertion cycles remains to be quantified.

VI. CONCLUSION

In this work, we introduced RAPID, a reconfigurable platform designed to accelerate multi-modal manipulation research. By mirroring mechanical modularity with software modality observability, we addressed the integration overhead that plagues iterative hardware design. Our system-centric evaluation demonstrated that RAPID reduces the time required for hardware reconfiguration by two orders of magnitude compared to traditional workflows and enables robust inference even when sensors are physically removed.

These results suggest that treating data collection interfaces as adaptive platforms rather than static devices is a viable path toward more rigorous real-world hardware–software co-design. We hope that by lowering the barrier to hardware iteration, RAPID will encourage the community to move beyond fixed benchmarks and explore the vast design space

of robot morphology and sensing. We have open-sourced the complete hardware design files and software stack to facilitate this transition.

In future work, we aim to address the remaining bottleneck of extrinsic calibration. While RAPID automates device discovery, the geometric alignment of new cameras currently requires manual recalibration. We plan to integrate marker-based self-calibration routines that trigger automatically upon module insertion, further closing the loop on fully autonomous reconfiguration.

ACKNOWLEDGMENTS

We thank Yun Gui and Longsheng Jiang for their valuable discussions, feedback, and support throughout this project.

REFERENCES

- [1] Christopher Agia, Rohan Sinha, Jingyun Yang, Zi-ang Cao, Rika Antonova, Marco Pavone, and Jeannette Bohg. Unpacking failure modes of generative policies: Runtime monitoring of consistency and progress. *arXiv preprint arXiv:2410.04640*, 2024.
- [2] Elie Aljalbout, Jiaxu Xing, Angel Romero, Iretiayo Akinola, Caelan Reed Garrett, Eric Heiden, Abhishek Gupta, Tucker Hermans, Yashraj Narang, Dieter Fox, et al. The reality gap in robotics: Challenges, solutions, and best practices. *Annual Review of Control, Robotics, and Autonomous Systems*, 9, 2025.
- [3] Michal Bednarek, Piotr Kicki, and Krzysztof Walas. On robustness of multi-modal fusion—robotics perspective. *Electronics*, 9(7):1152, 2020.
- [4] Jagdeep Bhatia, Holly Jackson, Yunsheng Tian, Jie Xu, and Wojciech Matusik. Evolution gym: A large-scale benchmark for evolving soft robots. *Advances in Neural Information Processing Systems*, 34:2201–2214, 2021.
- [5] Raunaq Mahesh Bhirangi. *Tactile sensing for Robot Learning: Development to Deployment*. PhD thesis, Carnegie Mellon University, 2024.
- [6] Luzius Brodbeck, Simon Hauser, and Fumiya Iida. Morphological evolution of physical robots through model-free phenotype development. *PloS one*, 10(6):e0128444, 2015.
- [7] Michael Burgess and Edward H Adelson. Grasp everything (get): 1-dof, 3-fingered gripper with tactile sensing for robust grasping. *arXiv preprint arXiv:2505.09771*, 2025.
- [8] Jiahang Cao, Qiang Zhang, Hanzhong Guo, Jiaxu Wang, Hao Cheng, and Renjing Xu. Modality-composable diffusion policy via inference-time distribution-level composition. *arXiv preprint arXiv:2503.12466*, 2025.
- [9] Tianjian Chen, Zhanpeng He, and Matei Ciocarlie. Hardware as policy: Mechanical and computational co-optimization using deep reinforcement learning. *arXiv preprint arXiv:2008.04460*, 2020.
- [10] Tianjian Chen, Zhanpeng He, and Matei Ciocarlie. Co-designing hardware and control for robot hands. *Science Robotics*, 6(54):eabg2133, 2021.
- [11] Yizhou Chen, Andrea Sipos, Mark Van der Merwe, and Nima Fazeli. Visuo-tactile transformers for manipulation. *arXiv preprint arXiv:2210.00121*, 2022.
- [12] Tailai Cheng, Kejia Chen, Lingyun Chen, Liding Zhang, Yue Zhang, Yao Ling, Mahdi Hamad, Zhenshan Bing, Fan Wu, Karan Sharma, et al. Tacumi: A multi-modal universal manipulation interface for contact-rich tasks. *arXiv preprint arXiv:2601.14550*, 2026.
- [13] Cheng Chi, Siyuan Feng, Yilun Du, Zhenjia Xu, Eric Cousineau, Benjamin Burchfiel, and Shuran Song. Diffusion policy: Visuomotor policy learning via action diffusion. In *Proceedings of Robotics: Science and Systems (RSS)*, 2023.
- [14] Cheng Chi, Zhenjia Xu, Chuer Pan, Eric Cousineau, Benjamin Burchfiel, Siyuan Feng, Russ Tedrake, and Shuran Song. Universal manipulation interface: In-the-wild robot teaching without in-the-wild robots. In *Proceedings of Robotics: Science and Systems (RSS)*, 2024.
- [15] HeeSun Choi, Cindy Crump, Christian Duriez, Asher Elmquist, Gregory Hager, David Han, Frank Hearl, Jessica Hodgins, Abhinandan Jain, Frederick Leve, et al. On the use of simulation in robotics: Opportunities, challenges, and suggestions for moving forward. *Proceedings of the National Academy of Sciences*, 118(1):e1907856118, 2021.
- [16] Alexandre Colle, Karen Donaldson, and Mauro Dragone. Co-design methodology for rapid prototyping of modular robots in care settings. *Frontiers in Robotics and AI*, 12:1581506, 2025.
- [17] Antoine Cully, Jeff Clune, Danesh Tarapore, and Jean-Baptiste Mouret. Robots that can adapt like animals. *Nature*, 521(7553):503–507, 2015.
- [18] Yuqing Du, Daniel Ho, Alex Alemi, Eric Jang, and Mohi Khansari. Bayesian imitation learning for end-to-end mobile manipulation. In *International Conference on Machine Learning*, pages 5531–5546. PMLR, 2022.
- [19] Zipeng Fu, Tony Z Zhao, and Chelsea Finn. Mobile ALOHA: Learning bimanual mobile manipulation with low-cost whole-body teleoperation. In *Conference on Robot Learning (CoRL)*, 2024.
- [20] Huy Ha, Yihuai Gao, Zipeng Fu, Jie Tan, and Shuran Song. Umi on legs: Making manipulation policies mobile with manipulation-centric whole-body controllers. *arXiv preprint arXiv:2407.10353*, 2024.
- [21] Zihao He, Hongjie Fang, Jingjing Chen, Hao-Shu Fang, and Cewu Lu. Foar: Force-aware reactive policy for contact-rich robotic manipulation. *IEEE Robotics and Automation Letters*, 2025.
- [22] David Howard, Agoston E Eiben, Danielle Frances Kennedy, Jean-Baptiste Mouret, Philip Valencia, and Dave Winkler. Evolving embodied intelligence from materials to machines. *Nature Machine Intelligence*, 1(1):12–19, 2019.
- [23] Sylvain Koos, Jean-Baptiste Mouret, and Stéphane Doncieux. The transferability approach: Crossing the reality

gap in evolutionary robotics. *IEEE Transactions on Evolutionary Computation*, 17(1):122–145, 2012.

[24] Sam Kriegman, Amir Mohammadi Nasab, Dylan Shah, Hannah Steele, Gabrielle Branin, Michael Levin, Josh Bongard, and Rebecca Kramer-Bottiglio. Scalable sim-to-real transfer of soft robot designs. *arXiv preprint arXiv:1911.10290*, 2019.

[25] Mike Lambeta, Po-Wei Chou, Stephen Tian, Brian Yang, Benjamin Maloon, Victoria Rose Most, Dave Stroud, Raymond Santos, Ahmad Byagowi, Gregg Kammerer, et al. Digit: A novel design for a low-cost compact high-resolution tactile sensor with application to in-hand manipulation. *IEEE Robotics and Automation Letters*, 5(3):3838–3845, 2020.

[26] Maria Larsson, Hironori Yoshida, Nobuyuki Umetani, and Takeo Igarashi. Tsugite: Interactive design and fabrication of wood joints. In *UIST*, volume 20, pages 317–327, 2020.

[27] Guan-Horng Liu, Avinash Siravuru, Sai Prabhakar, Manuela Veloso, and George Kantor. Learning end-to-end multimodal sensor policies for autonomous navigation. In *Conference on robot learning*, pages 249–261. PMLR, 2017.

[28] Kevin Sebastian Luck, Heni Ben Amor, and Roberto Calandra. Data-efficient co-adaptation of morphology and behaviour with deep reinforcement learning. In *Conference on Robot Learning*, pages 854–869. PMLR, 2020.

[29] Raymond Ma and Aaron Dollar. Yale openhand project: Optimizing open-source hand designs for ease of fabrication and adoption. *IEEE Robotics & Automation Magazine*, 24(1):32–40, 2017.

[30] Steven Macenski, Tully Foote, Brian Gerkey, Chris Lalancette, and William Woodall. Robot operating system 2: Design, architecture, and uses in the wild. *Science Robotics*, 7(66):eabm6074, 2022. doi: 10.1126/scirobotics.abm6074.

[31] MSS Malik, Nabila Naz, Mubashir Gulzar, and Soumya K Manna. A scalable pneumatic soft gripper with modular silicone fingers for adaptive grasping. *Journal of Robotics*, 2025(1):9148351, 2025.

[32] Andrew Melnik, Luca Lach, Matthias Plappert, Timo Korthals, Robert Haschke, and Helge Ritter. Using tactile sensing to improve the sample efficiency and performance of deep deterministic policy gradients for simulated in-hand manipulation tasks. *Frontiers in Robotics and AI*, 8:538773, 2021.

[33] Rodrigo Moreno and Andres Faiña. Emerge modular robot: A tool for fast deployment of evolved robots. *Frontiers in Robotics and AI*, 8:699814, 2021.

[34] Natalia Neverova, Christian Wolf, Graham Taylor, and Florian Nebout. Moddrop: adaptive multi-modal gesture recognition. *IEEE Transactions on Pattern Analysis and Machine Intelligence*, 38(8):1692–1706, 2015.

[35] Tønnes F Nygaard, Charles P Martin, Eivind Samuelsen, Jim Torresen, and Kyrre Glette. Real-world evolution adapts robot morphology and control to hardware limitations. In *Proceedings of the Genetic and Evolutionary Computation Conference*, pages 125–132, 2018.

[36] Moises Pacheco, Rune Fogh, Henrik Hautop Lund, and David Johan Christensen. Fable ii: Design of a modular robot for creative learning. In *2015 IEEE international conference on robotics and automation (ICRA)*, pages 6134–6139. IEEE, 2015.

[37] Omar Rayyan, John Abanes, Mahmoud Hafez, Anthony Tzes, and Fares Abu-Dakka. Mv-umi: A scalable multi-view interface for cross-embodiment learning. *arXiv preprint arXiv:2509.18757*, 2025.

[38] Ralf Römer, Adrian Kobras, Luca Worbis, and Angela P Schoellig. Failure prediction at runtime for generative robot policies. *arXiv preprint arXiv:2510.09459*, 2025.

[39] Kent Rosser, Jia Kok, Javaan Chahl, and Josh Bongard. Sim2real gap is non-monotonic with robot complexity for morphology-in-the-loop flapping wing design. In *2020 IEEE International Conference on Robotics and Automation (ICRA)*, pages 7001–7007. IEEE, 2020.

[40] Siqi Shang, Mingyo Seo, Yuke Zhu, and Lillian Chin. Forte: Tactile force and slip sensing on compliant fingers for delicate manipulation. *arXiv preprint arXiv:2506.18960*, 2025.

[41] Karl Sims. Evolving virtual creatures. In *Seminal Graphics Papers: Pushing the Boundaries, Volume 2*, pages 699–706. 2023.

[42] Taku Sugiyama, Kyo Kutsuzawa, Dai Owaki, Elijah Almanzor, Fumiya Iida, and Mitsuhiro Hayashibe. Versatile graceful degradation framework for bio-inspired proprioception with redundant soft sensors. *Frontiers in Robotics and AI*, 11:1504651, 2025.

[43] Yikai Tang, Haoran Geng, Sheng Zang, Pieter Abbeel, and Jitendra Malik. Visual-geometry diffusion policy: Robust generalization via complementarity-aware multimodal fusion. *arXiv preprint arXiv:2511.22445*, 2025.

[44] Tarik Tosun, Jay Davey, Chao Liu, and Mark Yim. Design and characterization of the ep-face connector. In *2016 IEEE/RSJ International Conference on Intelligent Robots and Systems (IROS)*, pages 45–51. IEEE, 2016.

[45] Pankhuri Vanjani, Paul Mattes, Xiaogang Jia, Vedant Dave, and Rudolf Lioutikov. Disdp: Robust imitation learning via disentangled diffusion policies. In *Reinforcement Learning Conference*, 2025.

[46] Philipp Wu, Fred Shentu, Xingyu Lin, and Pieter Abbeel. Gello: A general, low-cost, and intuitive teleoperation framework for robot manipulators. In *Towards Generalist Robots: Learning Paradigms for Scalable Skill Acquisition @ CoRL2023*, 2023.

[47] Chen Xu, Tony Khuong Nguyen, Emma Dixon, Christopher Rodriguez, Patrick Miller, Robert Lee, Paarth Shah, Rares Ambrus, Haruki Nishimura, and Masha Itkina. Can we detect failures without failure data? uncertainty-aware runtime failure detection for imitation learning policies. *arXiv preprint arXiv:2503.08558*, 2025.

[48] Mengda Xu, Han Zhang, Yifan Hou, Zhenjia Xu, Linxi

Fan, Manuela Veloso, and Shuran Song. Dexumi: Using human hand as the universal manipulation interface for dexterous manipulation. *arXiv preprint arXiv:2505.21864*, 2025.

[49] Yue Xu, Litao Wei, Pengyu An, Qingyu Zhang, and Yong-Lu Li. exumi: Extensible robot teaching system with action-aware task-agnostic tactile representation. *arXiv preprint arXiv:2509.14688*, 2025.

[50] Wenzhen Yuan, Siyuan Dong, and Edward H Adelson. Gelsight: High-resolution robot tactile sensors for estimating geometry and force. *Sensors*, 17(12):2762, 2017.

[51] Tony Z Zhao, Vikash Kumar, Sergey Levine, and Chelsea Finn. Learning fine-grained bimanual manipulation with low-cost hardware. *arXiv preprint arXiv:2304.13705*, 2023.

[52] Zhaxizhuom Zhaxizhuoma, Kehui Liu, Chuyue Guan, Zhongjie Jia, Ziniu Wu, Xin Liu, Tianyu Wang, Shuai Liang, Pengan CHEN, Pingrui Zhang, et al. Fastumi: A scalable and hardware-independent universal manipulation interface with dataset. In *Conference on Robot Learning*, pages 3069–3093. PMLR, 2025.

[53] Brianna Zitkovich, Tianhe Yu, Sichun Xu, Peng Xu, Ted Xiao, Fei Xia, Jialin Wu, Paul Wohlhart, Stefan Welker, Ayzaan Wahid, et al. Rt-2: Vision-language-action models transfer web knowledge to robotic control. In *Conference on Robot Learning*, pages 2165–2183. PMLR, 2023.

APPENDIX

A. Physical Mask Data Format

The main text describes the Physical Mask as a “JSON dictionary.” For clarity, we provide detailed specifications of both the actual runtime format and the debug format:

Binary Format (Runtime). The production system publishes the Physical Mask at 500 Hz via shared memory (`/dev/shm/rapid.hardware_mask`) for minimal latency. The binary layout is cache-line aligned (32 bytes):

TABLE III

PHYSICAL MASK BINARY FORMAT (32 BYTES, CACHE-LINE ALIGNED).

Offset	Size	Field	Description
0	4	magic	0x52415044 (“RAPD”)
4	1	version	Protocol version (1)
5	1	device_count	Number of registered devices
6	2	_padding	Alignment padding
8	8	mask	Online status bitmask (u64)
16	8	timestamp_ns	Nanosecond timestamp
24	8	sequence	Monotonic sequence number

JSON Format (Debug). For debugging and visualization, a separate process outputs a human-readable JSON file at 1 Hz to `/dev/shm/rapid.hardware_mask.json`:

```
{
  "timestamp": "2026-02-05T10:30:00Z",
  "device_count": 3,
  "online_count": 2,
  "mask": "0x05",
  "mask_binary": "00000101",
  "sequence": 123456,
  "devices": [
    {"name": "cam_wrist",
     "bit": 0, "online": true},
    {"name": "tac_left",
     "bit": 1, "online": false},
    {"name": "motor_grip",
     "bit": 2, "online": true}
  ]
}
```

B. Device Discovery Pipeline

The discovery pipeline employs a two-tier matching strategy:

- 1) **Exact match:** VID + PID + Serial number uniquely identifies a specific device instance (e.g., a particular tactile sensor).
- 2) **Model match:** VID + PID identifies the device type when serial numbers are unavailable or for interchangeable devices.

Device registration is specified via TOML configuration files:

```
[device.tactile_left]
vid = "0x1234"
pid = "0x5678"
serial = "TACL001"
node = "tactile_publisher"
topic = "/rapid/tactile/left"
```

The registration script automatically generates udev rules (e.g., `/etc/udev/rules.d/99-rapid.rules`) to create stable symlinks such as `/dev/rapid/tactile_left`.

C. System Latency Analysis

Table IV summarizes the end-to-end latency from hardware event to software response.

TABLE IV
SYSTEM LATENCY BREAKDOWN FOR DEVICE HOT-PLUG EVENTS.

Stage	Latency
USB insertion → OS udev event	50–100 ms
udev event → process startup	100–200 ms
Process startup → data stream ready	800 ms–1.5 s
End-to-end (USB → visualization)	1.0–1.8 s

The “process startup to data stream ready” latency is device-dependent: USB cameras typically initialize within 800 ms, while network-connected devices (e.g., GoPro via USB-LAN adapter) may require up to 1.5 s. The Physical Mask itself is updated at 500 Hz (2 ms interval), ensuring that modality presence information is available with minimal delay after the OS-level event.

D. Driver Implementation

The device management system is implemented as a Rust daemon (`rapid_driver`) that monitors USB events, manages sensor processes, and publishes the Physical Mask to shared memory.

Shared Memory Mask Publishing. The Physical Mask is published at 500 Hz to `/dev/shm/rapid.hardware_mask` as a 32-byte, cache-line aligned binary structure (Table III). The structure uses a magic number (0x52415044, “RAPD”) for validation, a monotonic sequence number for detecting stale reads, and nanosecond timestamps for synchronization. The 64-bit mask field supports up to 64 independently tracked devices. A separate JSON file is published at 1 Hz for debugging and visualization purposes (Figure 6).

Hot-Plug Event Handling. Device lifecycle management is driven by udev events from the Linux kernel. When a USB device is inserted, the daemon extracts its identity (VID, PID, serial number) and performs two-pass matching against the registry:

- 1) **Exact match:** VID + PID + serial number uniquely identifies a specific device instance.
- 2) **Model match:** VID + PID alone identifies interchangeable devices when serial numbers are unavailable.

Upon successful match, the daemon spawns the configured `on_attach` command (typically a ZeroMQ publisher node) as a child process with its own process group. A 2-second cooldown prevents rapid reconnection loops from USB electrical bounce.

Graceful Process Termination. When a device is unplugged, the daemon terminates the associated process using a

Fig. 6. Terminal interface showing Physical Mask monitor with real-time device status, bitmask visualization, and process logs. Each device displays connection state (green: online, yellow: USB connected but process starting, red: offline) and assigned bit position.

graceful shutdown sequence: SIGTERM is sent to the process group, followed by a 5-second grace period for cleanup. If the process does not exit within this window, SIGKILL is issued to force termination. An optional `on_detach` command can be specified for additional cleanup (e.g., releasing network resources). Crashed processes are automatically restarted with exponential backoff (up to 5 attempts within 60 seconds) if the USB device remains connected.

Data Recording and Visualization. Sensor data streams are recorded in MCAP format, an open-source container format designed for robotics data. MCAP provides efficient columnar storage, random-access playback, and native support for ROS-style messages. The recorded data can be directly loaded into Foxglove Studio for multi-modal visualization (Figure 7), enabling synchronized playback of camera feeds, tactile images, and robot state. This recording pipeline captures the Physical Mask alongside sensor data, allowing offline analysis of how modality availability affects policy behavior.

E. Dataset Statistics

TABLE V
DATASET STATISTICS FOR THE TACTILE IDENTIFICATION TASK.

Parameter	Value
Total episodes	72
Episodes per configuration	36
Frames per episode	~100–170

The dataset comprises demonstrations collected with two block types (triangular and hexagonal texture), with 36 episodes per type. Episodes vary in length depending on grasp timing and placement trajectory.

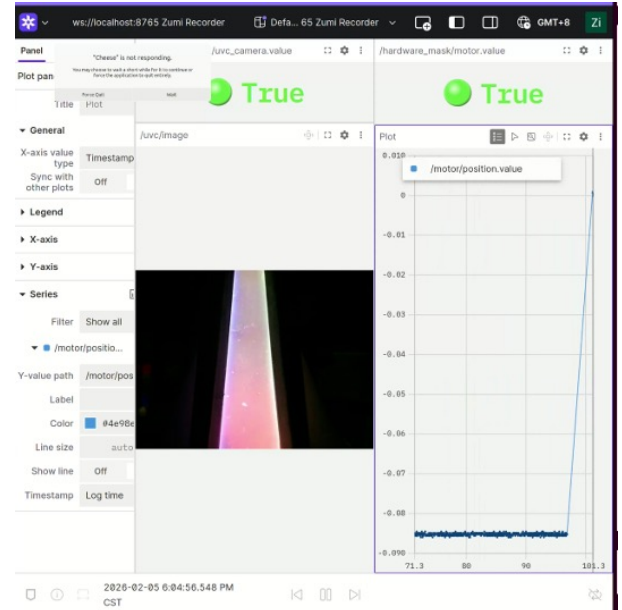


Fig. 7. Foxglove Studio visualization of MCAP-recorded session showing synchronized multi-modal data: wrist camera view, tactile sensor images, and robot joint states. The timeline enables scrubbing through recorded episodes for analysis and debugging.

TABLE VI
DIFFUSION POLICY HYPERPARAMETERS.

Parameter	Value
Architecture	CNN-based Diffusion Policy
Observation horizon	2
Action horizon	8
Prediction horizon	16
Training epochs	200
Modality dropout rate	0.3

F. Diffusion Policy Configuration

G. Ablation Study: Modality Configurations

Table VII presents ablation experiments investigating the contribution of different input modalities.

TABLE VII
ABLATION STUDY ON MODALITY CONFIGURATIONS.

#	Config	Data	Drop	Result
1	Vision only	mix	—	Biased (0.50)
2	Vision + mask	mix	0.3	Biased (0.50)
3	Vis + mask + diff	mix	0.3	Success (1.00)
4	Vision + diff	big	—	Biased (0.50)
5	Vision + diff	mix	—	Success (1.00)

Data: mix = mixture, big = bigcube. All diff image experiments use hand_view. “Biased” = policy places all objects to the same side; “Success” = correct texture-based placement.

Key findings:

- **Experiments 1–2:** Vision alone cannot discriminate objects that appear identical but differ in tactile texture.
- **Experiments 3, 5:** The diff image effectively captures

tactile-induced visual changes, enabling successful texture identification.

- **Experiment 4 vs. 5:** Dataset diversity (mixture vs. single configuration) affects policy generalization; training on a single cube size leads to biased behavior.

H. Diff Image Computation

The diff image captures visual changes induced by tactile contact:

$$\text{diff} = \frac{\text{current_frame} - \text{reference_frame}}{2} + 0.5 \quad (1)$$

where `reference_frame` is the first frame of the episode (before contact). The output is normalized to $[0, 1]$, with 0.5 representing no change. This encoding preserves both positive and negative intensity changes while maintaining a consistent input range for the policy network.

To verify that tactile images contain discriminative texture information, we trained a standalone classifier on tactile frames.

TABLE VIII
TACTILE TEXTURE CLASSIFICATION RESULTS.

Metric	Value
Architecture	ResNet-18 (ImageNet pretrained)
Dataset split	Episode-level (80/10/10)
Test accuracy	99.73%
Precision (triangular / hexagonal)	1.000 / 0.994
Recall (triangular / hexagonal)	0.995 / 1.000

Confusion Matrix:

	Pred: Triangular	Pred: Hexagonal
True: Triangular	586	3
True: Hexagonal	0	536

The near-perfect classification accuracy confirms that tactile images capture sufficient information to discriminate the two textures. This validates that the policy’s inability to distinguish textures in vision-only conditions (Table VII, Experiments 1–2) stems from the visual similarity of the blocks rather than insufficient tactile information in the diff images.

Table IX lists the hardware modules used in this work. Sensor-bearing modules provide YAML descriptors for automatic discovery; mechanical-only modules require no software configuration.

TABLE IX
RAPID MODULE CATALOG.

Module	Slot	Sensors	Bring-up
Finger (parallel-jaw)	front	–	–
Finger (pinch)	front	–	–
Rigid tip (PLA)	tip	–	–
Soft tip (TPU)	tip	–	–
Tactile tip (GET)	tip	cam+LED	USB
Wrist mount (std)	top	GoPro	Net
Wrist mount (angled)	top	GoPro	Net
Handheld adapter	bottom	–	–
Robot adapter	bottom	–	–

Slots: front (finger bodies), tip (fingertips), top (wrist mounts), bottom (adapters). Sensor-bearing modules provide YAML descriptors for automatic discovery; mechanical-only modules require no software configuration.